Survey of precursors to $P'P'$: Fine structure of mantle discontinuities

Fei Xu and John E. Vidale
Department of Earth and Space Science, University of California, Los Angeles, California, USA

Paul S. Earle
U.S. Geological Survey, Golden, Colorado, USA

Received 27 July 2001; revised 6 March 2002; accepted 3 October 2002; published 16 January 2003.

[1] The jumps in seismic velocity and density near 410- and 660-km depths have been postulated to mark phase changes in a locally, chemically homogeneous mantle. Seismic estimates of upper mantle discontinuity thickness and lateral variability have varied, posing difficulties for assessing models with chemical and phase transition layering. Observations of underside high-frequency ($\sim$1 Hz) P wave reflections from the 410- and 660-km discontinuity that precede the $P'P'$ phase provide unique constraints on the physical properties of these dynamically critical features. We have collected high-quality recordings of $P'P'$ and its precursors from three sources: the California Seismic Network, the Large Aperture Seismic Array in Montana, and the Global Seismic Network. The array and regional network data have great sensitivity to weak $P'P'$ precursors, whereas the global network recordings have good geographical distribution of bounce points. The only consistently observed reflections originate from depths near 410 km and 660 km. The reflector observed near 520-km depth with longer period waves, which has been interpreted as the olivine $\beta-\gamma$ phase transition, is too small in impedance contrast or too thick to reflect 1-Hz P waves. Data from all three networks indicate that the 1-Hz P waves from the "660" are bigger than those from the "410." Although large variability in $P'P'$ and its precursors' amplitudes prevents strong conclusions, we show that the $P'P'$ precursor amplitudes, travel time dispersion, and frequency content are consistent with a sharp ($\leq$2 km) 660 and a more diffuse 410, consistent with mineral physics predictions.
INDEX TERMS: 7203 Seismology: Body wave propagation; 7207 Seismology: Core and mantle; 7218 Seismology: Lithosphere and upper mantle; *KEYWORDS:* seismology, reflection, mantle, discontinuities

Citation: Xu, F., J. E. Vidale, and P. S. Earle, Survey of precursors to $P'P'$: Fine structure of mantle discontinuities, *J. Geophys. Res.*, *108*(B1), 2024, doi:10.1029/2001JB000817, 2003.

1. Introduction

[2] The structure of the upper mantle discontinuities is an important clue to the petrological makeup of the mantle and the Earth's dynamic behavior [*Shearer*, 1995]. The two major seismic discontinuities in the upper mantle, the "410" and the "660," are near depths of 410 km and 660 km, respectively. Many other boundaries have been reported, but these are smaller or less globally pervasive [*Bina*, 1991].

[3] The 410 is attributed to the olivine $\alpha-\beta$ phase transition [*Bina*, 1991; *Katsura and Ito*, 1989; *Ringwood*, 1969]. The 660 is widely accepted to mark the γ spinel to peroversuskite + magnesiowustite phase transition [*Chudinovskikh and Boehler*, 2001; *Ito and Takahashi*, 1989; *Shim et al.*, 2001]. The increase in seismic velocity and density at the 660 is interpreted to occur at <2 km [*Benz and Vidale*, 1993; *Husebye et al.*, 1977; *Sobel*, 1978; *Whitcomb and Anderson*, 1970]. However, the width of the 660 is too small to be resolved experimentally, and the precision of experimental measurements of pressure is comparable to seismically estimated width (2 km or 0.08 GPa) [*Stixrude*, 1997]. The sharpness (thickness of the velocity transition) of the 410 is less constrained. Mineral physics predictions of the width of the 410 vary, ranging from 11 to 19 km [*Akaogi et al.*, 1989; *Katsura and Ito*, 1989].

[4] Compositional variation across the discontinuities has also been suggested many times, perhaps in addition to phase changes. One argument for compositional variation has been the inability of phase changes alone to account for seismic observations. Thus we are motivated to look carefully at the seismic structure of the discontinuities.

[5] Numerous seismic investigations of upper mantle discontinuities between 200- and 700-km depth have been made over the past 50 years utilizing a variety of refracted, converted, and reflected waves. Seismic studies generally assume linear gradients across the 410 and 660, although actual transitions are probably more complicated, but perhaps not seismically resolvable [*Helffrich and Bina*, 1994; *Stixrude*, 1997].

0148-0227/03/2001JB000817$09.00

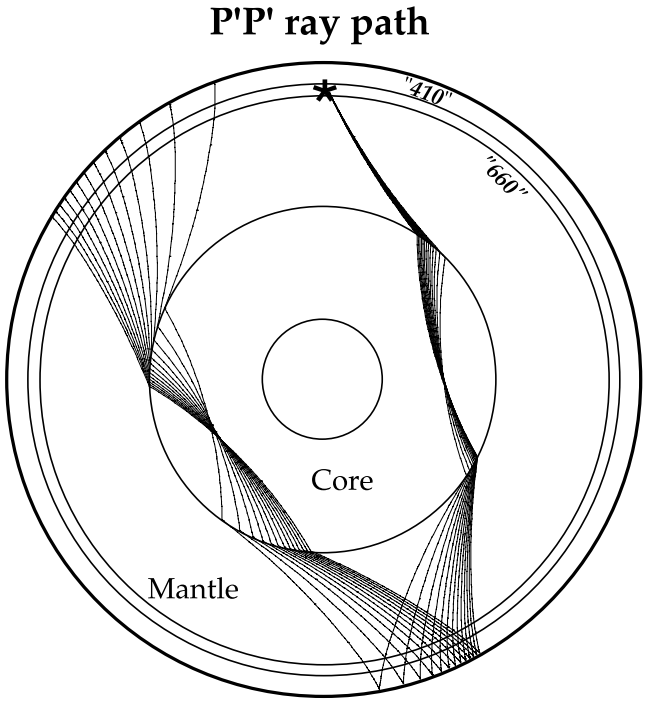

Figure 1. Ray paths of $P'P'$ (*PKPPKP*) from a 600-km-deep source. Arrivals from underside reflections of the 660 and the 410 near the bounce point are precursors.

[6] One method of detecting the presence and inferring the properties of a discontinuity uses triplicated body waves [*Grand and Helmberger*, 1984; *Melbourne and Helmberger*, 1998; *Vidale et al.*, 1995]. Measurement of the travel time curve triplication near its caustics can provide constraints on absolute velocity jumps across the discontinuities, but they are not sensitive to transition thicknesses below ~10-km width. *P*-to-*SV* and *SV*-to-*P* conversions at a discontinuity provide another way of measuring average boundary depth and its physical properties [*Niu and Kawakatsu*, 1995; *Shen et al.*, 1996; *Vidale and Benz*, 1992; *Wicks and Richards*, 1993] with less sensitivity to sharpness. Precursors to reflected phases such as *PP*, *SS* [*Flanagan and Shearer*, 1998a, 1998b; *Gu et al.*, 1998; *Shearer*, 1993; *Shearer and Flanagan*, 1999], and *ScS* reverberations [*Revenaugh and Jordan*, 1991a] are also used to probe the upper mantle discontinuities.

[7] This study, like numerous previous studies, uses high-frequency precursors to the reflected phase $P'P'$ (*PKPPKP*) to estimate discontinuity sharpness [*Adams*, 1971; *Benz and Vidale*, 1993; *Engdahl and Flinn*, 1969; *Nakanishi*, 1988; *Whitcomb and Anderson*, 1970]. Figure 1 shows ray paths for $P'P'$ and its precursors, which arrive ~40 min after the earthquake. It is best observed in the distance range 60°–75°. There, $P'P'$ provides a good signal-to-noise ratio because it arrives in a quiet interval on the seismogram and is amplified by a caustic near 71°. $P'P'$ precursors are commonly labeled as P'_dP', where d denotes the depth of the reflector. We refer to the underside reflections from the two main upper mantle discontinuities as $P'410P'$ and $P'660P'$, using the global-average depths of the discontinuities [*Revenaugh and Jordan*, 1991b; *Shearer and Masters*, 1992].

[8] Here we extend earlier work by studying $P'P'$ precursor recordings obtained from a search of all available data. We use the California Seismic Network (CSN), the Large Aperture Seismic Array (LASA) in Montana, and the Global Seismic Network (GSN). Although our coverage is far from ubiquitous, the $P'P'$ reflection points sample several tectonic settings. Velocity jumps and sharpness of the 410 and 660 are estimated by analyzing the frequency-dependent amplitudes of reflections assuming recent estimates of the impedance contrasts across the upper mantle discontinuities [*Shearer and Flanagan*, 1999].

2. $P'P'$ Precursor Observations at the Large Aperture Seismic Array and the California Seismic Network

[9] $P'410P'$ and $P'660P'$ are weak signals. We improve their signal-to-noise ratio by stacking seismograms from large-aperture arrays with many elements. We searched archives from two arrays, CSN and LASA (Figure 2) for observations of $P'P'$ precursors.

[10] The CSN (the combination of the Northern California Seismic Network and the Southern California Seismic Network) consists of more than 600 short-period vertical component seismometers across a 1100-km by 400-km area. The U.S. Geological Survey and California Institute of Technology began operating the CSN in triggered mode in the early 1970s and upgraded to continuous recording in the early 1990s. The CSN's large aperture allows for accurate slowness estimation and its large number of stations greatly reduces the largest sources of noise: microtremors and near-station reverberations.

[11] At full capacity the 200-km aperture LASA consisted of 525 seismometers arranged in twenty-one 8-km-wide subarrays. However, our data were collected later when about 300 stations were in operation. LASA's aperture is smaller than the CSN's, but its geometry, closely spaced

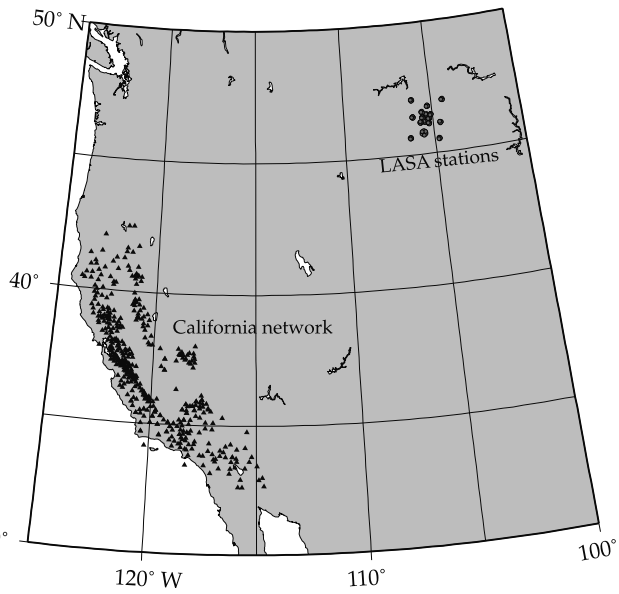

Figure 2. Locations of stations in the California Seismic Network and Large Aperture Seismic Array (LASA) used in this study.

Table 1. Events Recorded at the Large-Aperture Seismic Array (LASA) and the California Seismic Network (CSN)

Date	Time, UT	Latitude, °N	Longitude, °E	Depth, km	m_b	Trace[a]	Network
19 Jan. 1969	0702:04.4	44.01	143.17	204	6.3	333	LASA
5 Sept. 1971	1835:26.8	46.54	141.15	14	6.0	327	LASA
6 Sept. 1971	1337:10.1	46.76	141.39	21	6.3	319	LASA
27 Sept. 1971[b]	0559:55.8	73.39	54.92	0	6.5	325	LASA
12 Sept. 1973[b]	0659:54.3	73.30	55.16	0	6.8	340	LASA
27 Oct. 1973[b]	0659:58.0	70.80	53.96	0	6.9	342	LASA
29 Aug. 1974[b]	0959:56.2	73.39	54.92	0	6.4	204	LASA
9 Oct. 1974	0732:00.6	44.64	150.09	34	6.3	319	LASA
2 Nov. 1974[b]	0459:57.4	70.83	53.82	0	6.4	206	LASA
17 Oct. 1990	1430:14.9	−10.99	−70.78	616	6.5	111	CSN
24 May 1991	2050:55.4	−16.48	−70.72	126	6.3	107	CSN
6 July 1991	1219:45.7	−13.29	−72.42	105	6.1	103	CSN
9 June 1994	0033:13.0	−13.7	−67.3	637	6.9	219	CSN
9 Oct. 1994	0755:38.0	43.90	147.90	23	6.5	97	CSN

[a]Number of traces used in envelope stacks.
[b]Nuclear explosions.

stations, and uniform borehole instrumentation make this array ideal for studying low-amplitude, high-frequency $P'P'$ precursors.

[12] We selected all CSN and LASA data for m_b 6.0 and greater events with high signal-to-noise level $P'P'$ arrivals in the epicentral distance range 58°–78°. We found the five CSN earthquakes and nine LASA events (including five nuclear explosions) listed in Table 1. The $P'P'$ reflection points for the selected events cluster under the South Atlantic Ocean, Antarctica, and the Indian Ocean (Figure 3).

[13] Waveform stacking is essential in the identification of weak precursors to $P'P'$. It can effectively suppress the incoherent noise and allows for estimates of the slowness of each seismic phase. For our analysis, we obtain up to 300 seismograms for each LASA event and up to 600 seismograms for each CSN event. Seismograms with high signal-to-noise $P'P'$ phases and minimal coda were selected. Traces containing data spikes in the precursors' time window were discarded. We note that we may underestimate the amplitude of precursors because our selection process may be prejudiced in favor of anomalously large $P'P'$ arrivals. If we were to select some events with $P'P'$ amplified by focusing that does not affect the precursors, the precursors will appear unduly small. However, we noticed no events with an excellent $P'P'$-to-noise ratio without precursors.

[14] Band-pass filtering between 0.5 and 1.5 Hz was applied to the selected seismograms in order to obtain the best signal-to-noise ratio. Next we stacked envelopes of these band-pass-filtered traces for each event. A significant fraction of the $P'P'$ and precursor phases was not coherent, which is why we could not apply more powerful coherent stacking techniques.

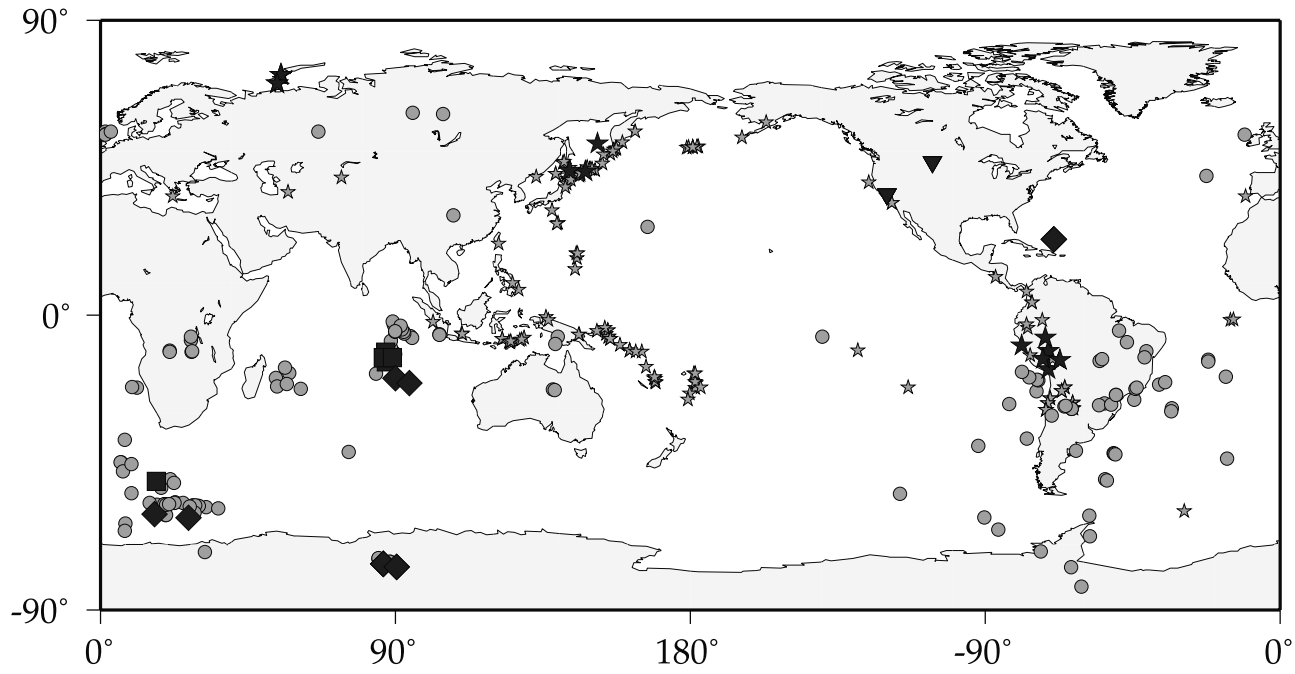

Figure 3. Bounce points of $P'P'$ (shaded circles, GSN traces; squares, California Seismic Network data; diamonds, LASA events). Bounce points of closely located events may appear overlapping. The source locations of these events are marked by stars (shaded stars, GSN data; solid stars, CSN and LASA data). Inverted triangles mark the locations of CSN and LASA.

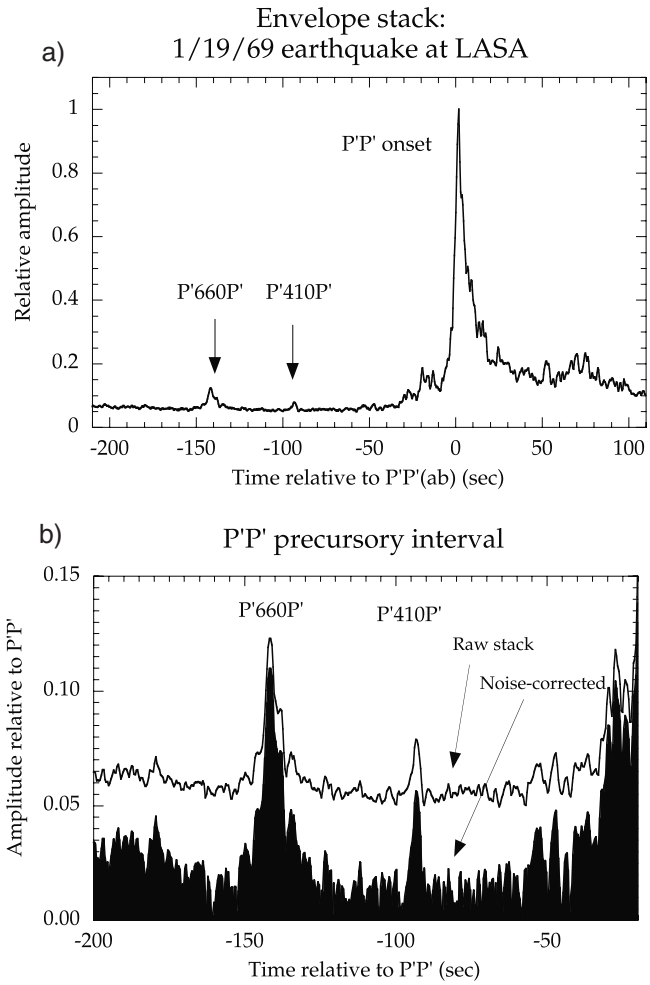

Figure 4. (a) Envelope stack for $P'P'$ and its precursors time window of the 19 January 1969 event (Table 1) recorded at LASA. The origin is the expected arrival time of $P'P'$, and the amplitude is normalized relative to the peak of $P'P'$. (b) Blowup of the precursory time window before $P'P'$. After correcting for noise, $P'410P'$ is about half the amplitude of $P'660P'$.

[15] Figure 4a shows the stacked seismograms of the 19 January 1969 event (see Table 1) for $P'P'$ and its precursory window. $P'410P'$ and $P'660P'$ precede $P'P'$ by 93 and 142 s, respectively. We correct for noise in the precursory window from 200 to 20 s before $P'P'$ based on two simple assumptions (Figure 4b): (1) Noise amplitude is constant, and (2) the amplitude of the $P'dP'$ signal S is the square root of the difference of the squares of the total amplitude A and noise N, i.e., $A^2 = N^2 + S^2$. Following these assumptions, the amplitudes of $P'660P'$ and $P'410P'$ are 12% and 6%, respectively, of that of $P'P'$.

[16] Further correction for attenuation is needed before we can model the ratios of $P'660P'/P'P'$ and $P'410P'/P'P'$ with velocity and density profiles across the discontinuities. For comparison, envelope-stacked seismograms of four LASA events and the average of these four events are plotted in Figure 5, including the 19 January 1969 event. Variations in the amplitudes of both $P'660P'$ and $P'410P'$ are apparent. However, in general, $P'410P'$ arrivals are small, whereas $P'660P'$ arrivals exist in all the envelope-stacked seismograms of our data. $P'660P'$ has about twice the amplitude of $P'410P'$, as indicated by the noise-corrected average of four events plotted at the bottom of Figure 5. Figure 6 also shows the same observation from envelope stacks of California network earthquakes. Recordings of five events and their average are constructed in the same manner.

3. Analysis of Global Seismic Network Data

[17] Seismograms from the GSN are another source of data in this study. With $P'P'$ and its precursors recorded by GSN stations around the world, a more global survey of reflections from upper mantle discontinuities is possible. The difficulty with single GSN stations is that the $P'660P'$ and $P'410P'$ precursors are only rarely identifiable above other signals and noise. Low signal-to-noise ratio and topography of the discontinuity surfaces [*Davis*, 1989] have been used to explain the rarity of confirmed $P'410P'$ and $P'660P'$ sightings on paths to Germany.

[18] In order to find seismograms with the highest signal-to-noise ratios in $P'P'$ and its precursory windows, we collected ~1200 vertical-component broadband records of

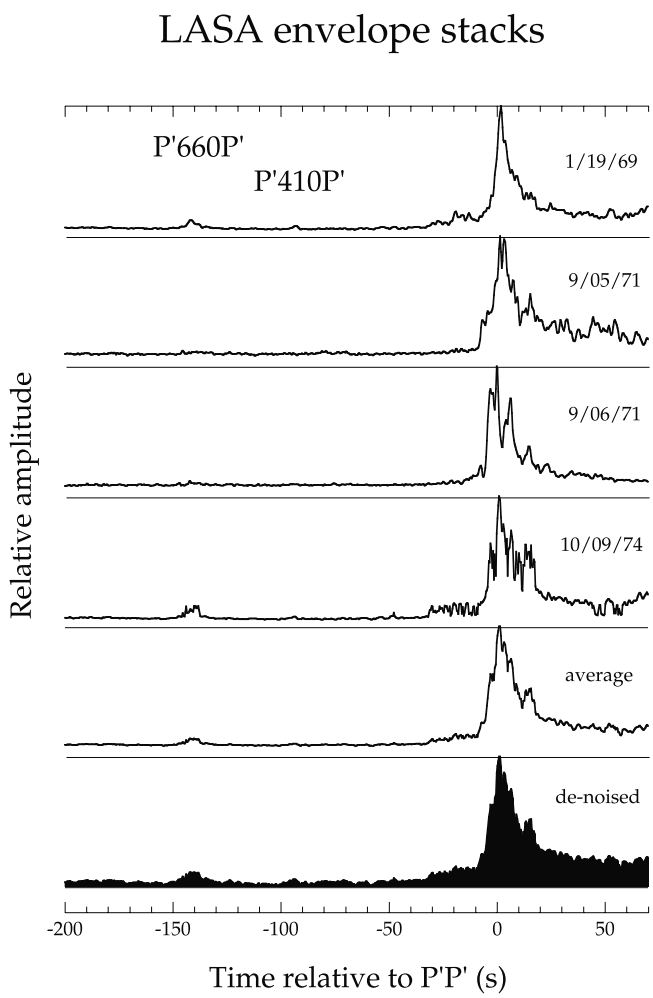

Figure 5. Envelope stacks of four LASA events and their average. The bottom plot represents the average of these four events after correcting for noise.

events larger than M_w 6.3 recorded in the distance range 67°–73°. To avoid signal-generated noise from the S wave coda and microseisms, we band-pass filter the broadband traces around 1-s period. We visually examine every trace and reject those that have low signal-to-noise ratios or protracted $P'P'$ codas. This reduces the data set to 91 seismograms. Four typical seismograms are shown in Figure 7. There is the suggestion of more energy in the expected arrival time of $P'660P'$ than elsewhere in the window preceding $P'P'$, but we stack to improve the resolution.

[19] The seismograms are shifted in time to align the $P'P'$ for all traces, the peak amplitude of $P'P'$ is normalized, and then the envelope of the traces are stacked. Figure 8 shows the envelope-stacked sum of the 91 traces. The background noise level is 14% of the peak amplitude of $P'P'$ from 200 until 50 s before $P'P'$. The signals arriving just before $P'P'$ are probably caused by asymmetric bounces in the uppermost mantle and crust. We remove background noise in Figure 8 with the same assumptions that are described in section 2; that is, it is a constant fraction (14% in this case) of the peak of $P'P'$ and is expected to contribute in a root-mean-square sense. An increase in the envelope amplitude is visible in Figure 8 at the expected arrival time for $P'660P'$ with about the same temporal shape as $P'P'$. No such increase is visible for $P'410P'$ even though a reflected arrival from the 410 as little as half the strength of that from the 660 would have been visible.

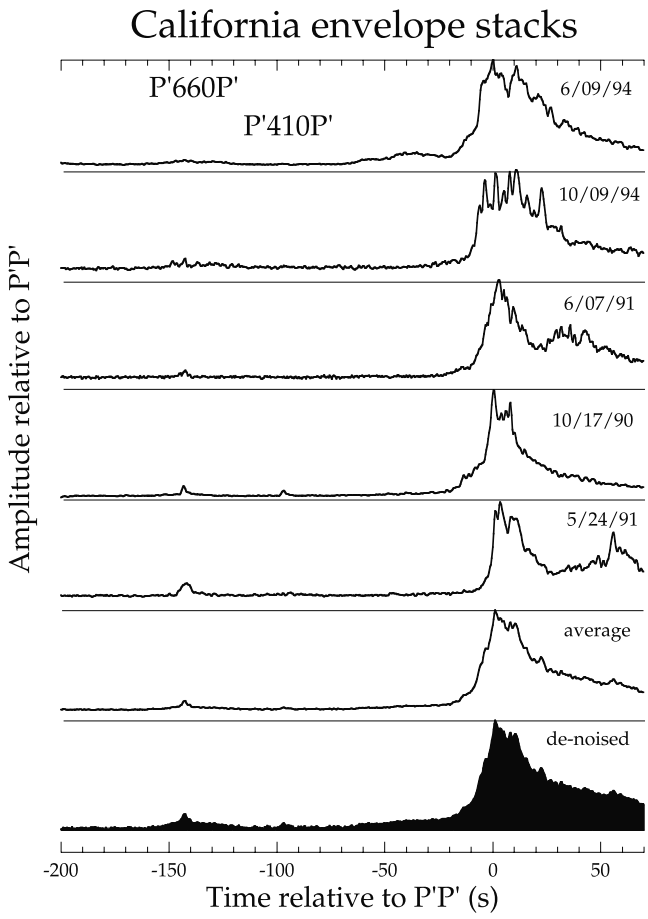

Figure 6. Envelope stacks of five California Seismic Network events as well as their average. The bottom plot represents the average of these five events after correcting for noise.

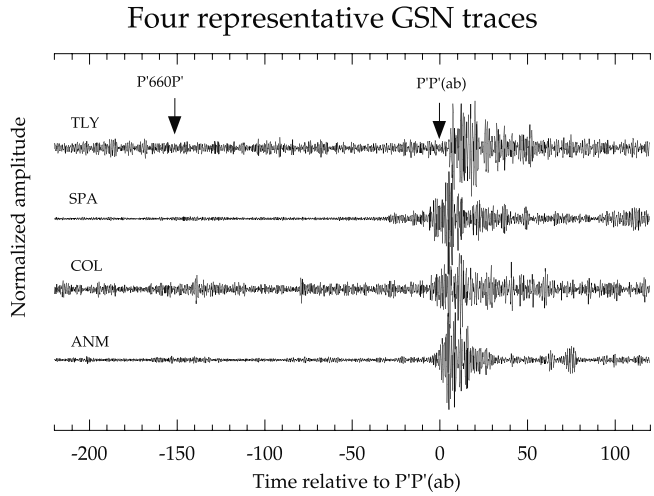

Figure 7. Four typical GSN Fast Archive Recovery Method (FARM) traces used in our stacking analysis. The predicted $P'P'$ arrival time (PREM) is the origin for the horizontal axis.

[20] The $P'P'$ reflection points of these 91 traces (from more than 70 earthquakes) are well-distributed around the globe and span several different tectonic settings (as shown by the shaded circles in Figure 3). The data were selected from the signal-to-noise ratios of $P'P'$ rather than its precursors. As described above, we expect the amplitude of the upper mantle discontinuity reflections to be slightly underestimated, since we will preferentially include anomalously large $P'P'$ arrivals. $P'660P'$ is ~15% as large as $P'P'$ in the raw stack. We will correct for attenuation in section 4. These global observations confirm that the 660 is generally much more reflective than the 410 for 1-s period P waves.

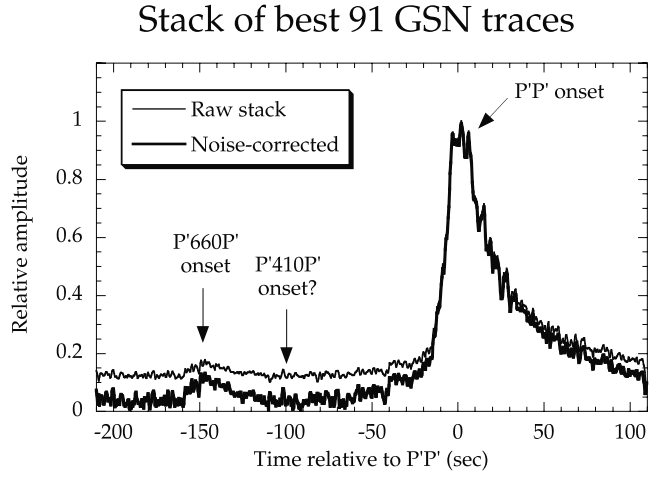

Figure 8. A stack of the envelopes of 91 GSN traces (thin line). Each trace is normalized before stacking. A stack of envelopes of these 91 traces after correction (thick line) for a noise level of 14% is also shown, as are the expected times of the onset of $P'660P'$ and $P'410P'$.

4. Discussion

[21] The most robust feature of all three data sets is the difference between the 410 and 660 reflection amplitudes, with $P'410P'$ being less than half the strength of $P'660P'$ (Figure 9). This is consistent with previous studies, which report more observations of $P'660P'$ than $P'410P'$ [*Sobel*, 1978]. The amplitude variability of $P'P'$ may be a factor of 10 [*Sobel*, 1978]. However, the amplitude ratios $P'660P'/P'P'$, $P'410P'/P'P'$, and $P'410P'/P'660P'$ in the stacked seismograms remain fairly constant in three independent data sets (Figure 9). This gives us an opportunity to infer the average physical properties, primarily the impedance, of upper mantle discontinuities.

[22] Our events span an epicentral distance range from 58° to 72°. Standard radial P velocity models predict that amplitudes of $P'P'$ and P'_dP' vary with distance, especially around the $P'P'$ caustic near 71°. However, stacked seismograms from events with different epicentral distances do not show trends with distance near the caustic. This defocusing of the caustic could arise from lateral variation of P velocity in the mid or lowermost mantle, in the core structure, or in the topography of the discontinuities. Thus our results are not greatly complicated by amplitude fluctuations caused by the caustic.

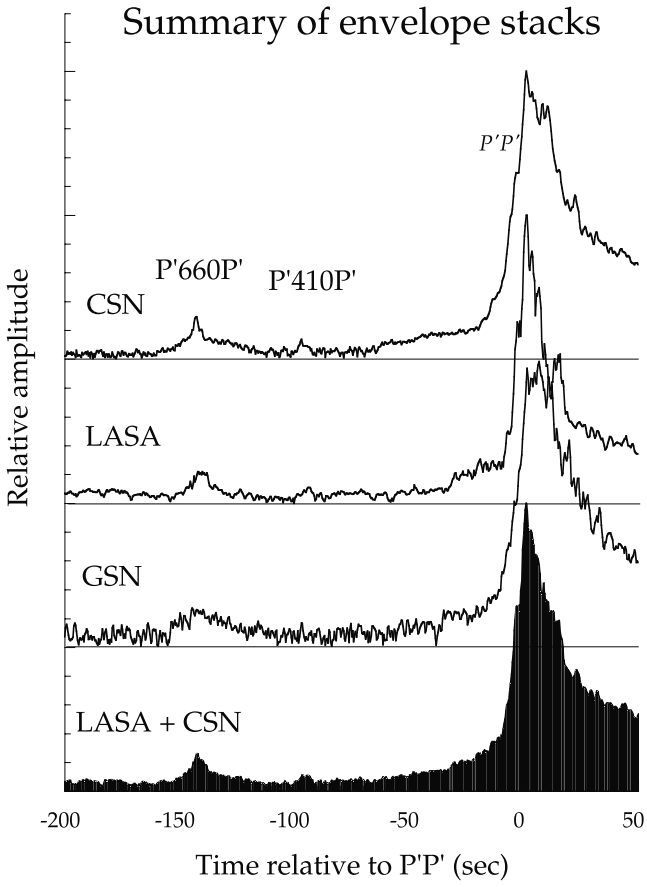

Figure 9. A summary of envelope stacks of our whole data set. CSN recordings, LASA recordings, GSN FARM data, and an average of LASA and CSN recordings are plotted. Note the consistency of $P'660P'$ and $P'410P'$ amplitudes among different data sets.

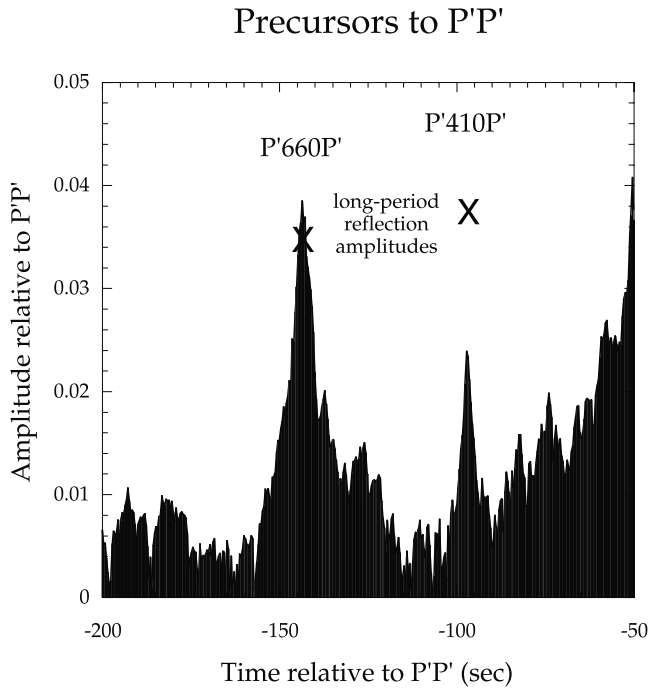

Figure 10. A stack of the network recordings, corrected for noise and attenuation. We selected the 14 events (including five nuclear tests) with the lowest noise before P′P′ from our collection of LASA and CSN data. The crosses show the predicted reflection coefficients from a recent model [*Shearer and Flanagan*, 1999]. We use a recent upper mantle attenuation model [*Warren and Shearer*, 2000].

[23] The data from the CSN and LASA are combined to estimate the average reflection coefficient of the 410 and 660. We corrected for the noise (as illustrated in Figure 4b) and P wave attenuation above the discontinuities with a recent attenuation model [*Warren and Shearer*, 2000]. Mantle attenuation has the effect of the surface-reflected $P'P'$ being more attenuated than the $P'660P'$ and $P'410P'$

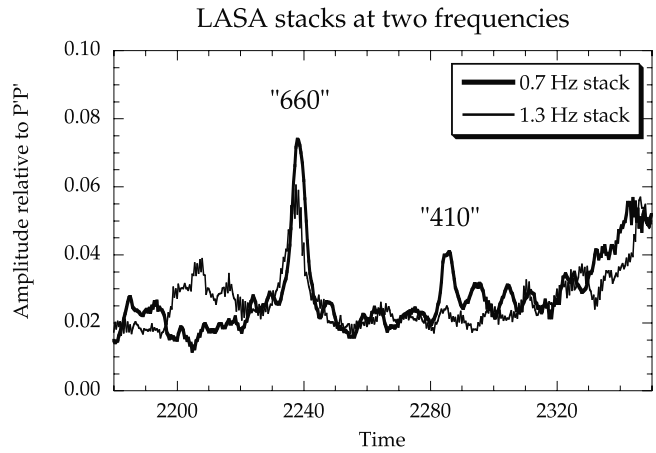

Figure 11. LASA stacks at two frequencies. Seismograms from nine LASA events are filtered in three different frequency bands at ~0.7 Hz and ~1.3 Hz. The averages of their envelope stacks are represented by traces with different line widths (a thinner line corresponds to a higher-frequency band).

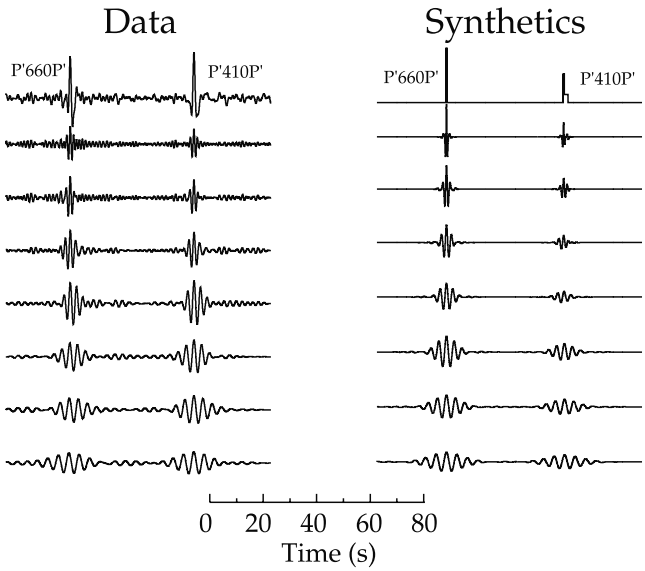

Figure 12. (left) Stacked trace of the 17 October 1990 event (Table 1) showing $P'410P'$ and $P'660P'$. $P'P'$ from this event bounces beneath the Indian Ocean. The stacked trace is band-pass-filtered around 1.0, 1.5, 2.0, 2.5, 3.0, 3.5, and 4.0 s. (right) Synthetics of P wave reflections off the models of the 410 and 660 shown in Figure 13. The synthetic traces are filtered the same way as the data stack. The source time function is a delta function in the calculation. Each trace is autoscaled.

phases, so the correction reduces the reflection amplitude. We obtained an amplitude ratio of ~3.9% for $P'660P''/P'P'$ and ~2.4% for $P'410P'/P'P'$ (Figure 10).

4.1. Comparison of Short- and Long-Period Reflections

[24] Evidence that the 660 is sharper than the 410 comes from the comparison of our high-frequency observations with the long-period study of *Shearer and Flanagan* [1999]. They constrain the average velocity and density changes across the 410 and 660 by observing the range dependence in long-period *PP* and *SS* precursors. We calculated the reflection coefficients of the 410 and 660 from their model. As indicated by the two crosses in Figure 10, the long-period model predicts reflection coefficients of 3.6% for the 660 and 3.9% for the 410 at the incident angle of $P'P'$.

[25] The amplitude of seismic energy reflecting from a small zero-thickness discontinuity depends on the angle of incidence and the impedance contrast across the boundary [*Aki and Richards*, 1980; *Richards*, 1972]. The impedance is the product of velocity and density across the boundary. For seismic waves reflecting from high-gradient zones the amplitude of reflected energy depends on the width of the zone and how the impedance change is distributed across the zone [*Aki and Richards*, 1980; *Richards*, 1972]. The amount of reflected energy diminishes rapidly when the width of the gradient zone exceeds a quarter wavelength of the incident P wave. Thus, in order to estimate the upper mantle discontinuities' sharpness from the observed reflection coefficients, one has to know or assume the total P impedance contrast and distribution across the boundaries.

[26] Only relatively sharp changes in impedance, primarily with wavelengths from 0 to 5 km, reflect 0.5 ~ 1.5 Hz P waves, whereas long-period P waves will effectively reflect off gradual transition layers up to 20 km thick. *Shearer and Flanagan*'s [1999] model predicts a 3.6% reflection from a zero-thickness 660 at $P'P'$ geometry. Consequently, the observed 3.9% reflected amplitude indicates that 660 is close to a zero-thickness transition. This suggests that the entire velocity jump across the 660 occurs within a few kilometers. Our data do not resolve the difference between a 2-km-thick transition and a zero-thickness discontinuity. A preliminary reference Earth model (PREM) and ak135 would require a broader 660 to explain the observed 3.9% reflection because they have a larger impedance contrast across the 660. However, regional reflection studies [*Estabrook and Kind*, 1996; *Grand and Helmberger*, 1984; *Shearer and Flanagan*, 1999; *Walck*, 1984] indicate that the impedance change across the 660 in PREM and ak135 is too large.

[27] On the other hand, there is a discrepancy between the high-frequency observation of $P'410P'/P'P'$ and its long-period prediction. $P'410P'/P'P'$ at high frequency is only ~60% of $P'410P'/P'P'$ at long period. These observations suggest that the 410 may be a combination of a sharp impedance change and a more gradual transition, which is

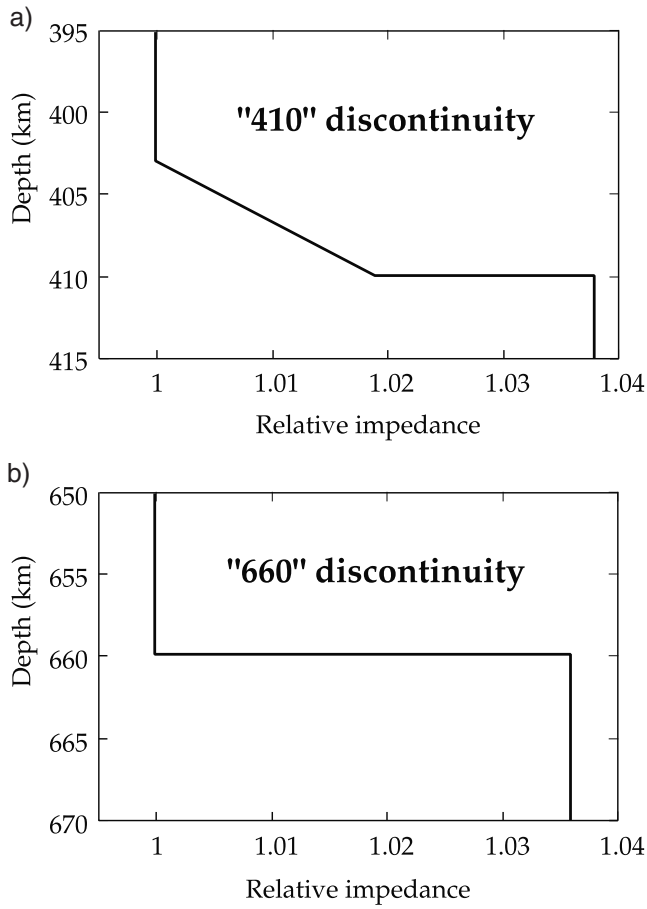

Figure 13. Simple models of the 410 and 660. (a) The 410 modeled as a combination of sharp transition (1.9% impedance contrast) and a gradual transition (7 km thick, 1.9% impedance contrast). (b) The 660 modeled as a sharp boundary with impedance contrast 3.6%.

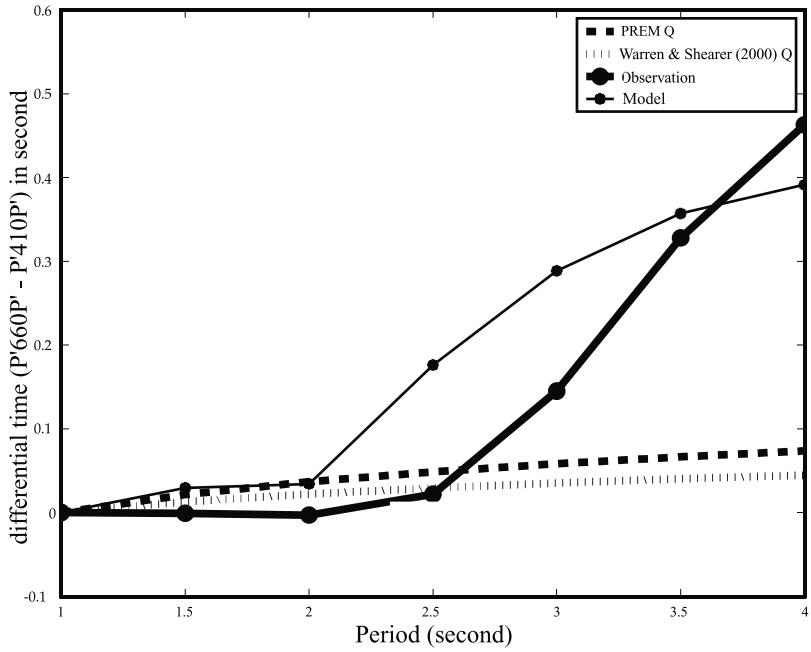

Figure 14. Differential travel time between $P'410P'$ and $P'660P'$ calculated by cross correlation at different periods relative to a 1-s period. The thick dotted line represents the data shown in Figure 12 (left), whereas the thin dotted line represents the synthetics data shown in Figure 12 (right). We also estimate the effect of attenuation on the differential travel time using two attenuation models [*Warren and Shearer*, 2000].

consistent with the structure of phase transitions predicted by equilibrium thermodynamics. Such predictions have most of the transition occurring in a narrow interval near the lower boundary of phase loop [*Stixrude*, 1997].

4.2. Dispersion and Frequency-Dependent Amplitude Ratios

[28] The observed 2.4% reflection from the 410 would match the prediction from the velocity and density jump across the 410 obtained by *Shearer and Flanagan*'s [1999] long-period study if the impedance change is spread linearly across ~10 km. However, we have two additional observations to constrain the velocity profile near a 410-km depth that necessitate a more complicated model: dispersion and evidence for frequency-dependent amplitudes. However, this additional evidence is less definitive than the amplitude ratios discussed in section 4.1.

[29] A seismic wave reflecting from a structure that consists of a sharp discontinuity or a linear gradient does not disperse. Reflected waves from a structure that consists of a sharp discontinuity and a gradual transition can be slightly dispersed. Within this range the high-frequency part of the wave would only see the sharp transition, whereas the low-frequency part would see the whole structure. Thus the travel time of a reflected wave may vary with its frequency.

[30] Also, variations in the amplitudes of $P'660P'$ and $P'410P'$ at different frequencies provide clues about the thicknesses of these two boundaries. However, only $P'P'$ precursors in the LASA recordings of large nuclear tests and the 17 October 1990 event had the bandwidth and signal-to-noise levels sufficient to measure frequency dependence. We applied narrow band-pass filters (centered at 0.7 and 1.3 Hz; quarter wavelength 3.6 and 1.9 km) to LASA events and coherently stacked the filtered traces. As Figure 11 shows, the amplitude of $P'660P'$ varies <20% in the above mentioned frequency bands, whereas the amplitude of $P'P'410P'$ is reduced with high-frequency $P'410P'$ dropping to the noise level. This suggests that the 410 is less sharp than the 660.

[31] We found only one event with $P'P'$ precursors that allowed us to analyze the subtle change in differential travel time between $P'410P'$ and $P'660P'$ as a function of frequency. Here, $P'660P'$ served as the reference phase. This magnitude 6.5 South American earthquake recorded by the California network has an anomalously large $P'410P'$ and has been used previously [*Benz and Vidale*, 1993] to argue for a locally simple and sharp 410. Figure 12 (left) shows the $P'P'$ precursory window of the slant-stacked trace of this quake and the filtered seismograms for seven 1-s-wide passbands.

[32] These data are best explained by a 410 model that combines a sharp jump with a 7-km gradual transition above it, as shown in Figure 13a. We do not have sufficient resolution to invert for a more detailed model of the 410. The sharp transition has an impedance contrast of 3.8%, and the overlying linear gradient change across 7 km also has an 3.8% impedance contrast. The 660 model (Figure 13b) invokes a sharp transition with an impedance contrast of 7.2%. The total impedance contrasts across the 410 and 660 used in this model are derived from a recent study of amplitude versus offset of long-period shear reflections [*Shearer and Flanagan*, 1999].

[33] We compute reflections off our simple model, also shown in Figure 12. The reflection in this model has an amplitude of 2.0% of the incident wave at 1 Hz. If values from Earth reference models such as PREM and ak135 are used, we will have only a slightly different 410 reflection

coefficient. This agreement is because both PREM [*Dziewonski and Anderson*, 1981] and ak135 include velocity and density changes at 410 similar to the preferred model of *Shearer and Flanagan* [1999].

[34] By cross correlation, we measure the differential travel time between $P'410P'$ and $P'660P'$ (at seven frequency bands) for both the data and the synthetic. As Figure 14 shows, the data and synthetic dispersion are consistent; both are 1 order of magnitude larger than the dispersion expected from attention models in the transitional upper mantle.

[35] We did not observe reflected energy from 520-km depth as has been seen in long-period *S* reflections [*Revenaugh and Jordan*, 1991a; *Shearer*, 1993]. The absence of $P'520P'$ at 1-Hz frequency indicates that the presumed $\beta-\gamma$ olivine phase change at 520 km is either too weak in *P* impedance contrast or too broad to reflect a high-frequency *P* wave. We also do not systematically observe reflections from other levels, such as 220-, 700-, or 910-km depths, despite their observation in other studies.

[36] The sharpness of phase transitions in the upper mantle is essentially described by the yield, or mole fraction, of the high-pressure phase as a function of the pressure [*Stixrude*, 1997]. Our preferred seismic model for the 410 is consistent with recent mineral physics studies [*Helffrich and Bina*, 1994; *Helffrich and Wood*, 1996; *Stixrude*, 1997], which indicate a nonlinear dependence of yield on pressure. Most of the transition occurs in a narrow interval near the lower boundary of the phase loop. The narrow width of the phase transition appears sharp in high-frequency reflection studies such as $P'P'$. However, the whole phase loop, 8–19 km in thickness [*Akaogi et al.*, 1989; *Katsura and Ito*, 1989], serves as a reflector for long-period *PP* and *SS*. The width of the phase transition can be substantially affected by the presence of a nontransforming phase. *Stixrude* [1997] predicts that the width of the olivine to wadsleyite transition in the presence of pyroxene and garnet is approximately half that of the binary phase loop at typical transition zone temperatures. This mechanism may resolve the discrepancy that the estimated thickness of the 410 based on its seismic reflectivity is too narrow to be explained by the equilibrium olivine to wadsleyite phase transition [*Benz and Vidale*, 1993]. Some of the variability in our 410 and 660 observations may be due to variations in temperature [*Bina and Helffrich*, 1994; *Helffrich and Bina*, 1994] or water content [*Helffrich and Wood*, 1996; *Wood*, 1995].

[37] The width of the 660, the transition from spinel to peroversuskite + magnesiowustite, is too small to resolve experimentally [*Stixrude*, 1997]. This constraint is consistent with our observation that the 660 is extremely sharp. So $P'P'$ precursor observations can be reconciled with laboratory experiments and do not require compositional variations nor unexpected details in the phase transitions at the 410 and 660.

[38] **Acknowledgments.** We thank Bob Woodward, the Albuquerque Seismological Laboratory, and Peter Davis for access to the LASA data and Rick Lester and Katrin Douglas for data from the California short-period data.

References

Adams, R. D., Reflections from discontinuities beneath Antarctica, *Bull. Seismol. Soc. Am.*, *61*, 1441–1451, 1971.

Akaogi, M., E. Ito, and A. Navrotsky, The olivine-modified spinel-spinel transitions in the system Mg_2SiO_4-Fe_2SiO_4 calorimetric measurements, thermochemical calculation, and geophysical application, *J. Geophys. Res.*, *94*, 15,671–15,685, 1989.

Aki, K. and P. G. Richards, *Quantitative Seismology: Theory and Methods*, 932 pp., W. H. Freeman, New York, 1980.

Benz, H. M., and J. E. Vidale, The sharpness of upper mantle discontinuities determined from high-frequency $P'P'$ precursors, *Nature*, *365*, 147–150, 1993.

Bina, C. R., Mantle discontinuities, *U.S. Natl. Rep. Int. Union Geod. Geophys. 1987–1990*, *Rev. Geophys.*, *29*, 783–793, 1991.

Bina, C. R., and G. Helffrich, Phase transition Clapeyron slopes and transition zone seismic discontinuity topography, *J. Geophys. Res.*, *99*, 15,853–15,860, 1994.

Chudinovskikh, L., and R. Boehler, High-pressure polymorphs of olivine and the 660-km seismic discontinuity, *Nature*, *411*, 574–577, 2001.

Davis, J. P., Precursors to $P'P'$ re-examined using broad-band data, *Geophys. J. Int.*, *99*, 595–604, 1989.

Dziewonski, A. M., and D. L. Anderson, Preliminary reference Earth model, *Phys. Earth Planet. Inter.*, *25*, 297–356, 1981.

Engdahl, E. R., and E. A. Flinn, Seismic waves reflected from discontinuities within Earth's upper mantle, *Science*, *163*, 177–179, 1969.

Estabrook, C. H., and R. Kind, The nature of the 660-kilometer upper-mantle seismic discontinuity from precursors to the *PP* phase, *Science*, *274*, 1179–1182, 1996.

Flanagan, M. P., and P. M. Shearer, Global mapping of topography on transition zone velocity discontinuities by stacking *SS* precursors, *J. Geophys. Res.*, *103*, 2673–2692, 1998a.

Flanagan, M. P., and P. M. Shearer, Topography on the 410-km seismic velocity discontinuity near subduction zones from stacking of *sS*, *sP*, and *Pp* precursors, *J. Geophys. Res.*, *103*, 21,165–21,182, 1998b.

Grand, S. P., and D. V. Helmberger, Upper mantle shear structure of North America, *Geophys. J. R. Astron. Soc.*, *76*, 399–438, 1984.

Gu, Y., A. M. Dziewonski, and C. B. Agee, Global de-correlation of the topography of transition zone discontinuities, *Earth Planet. Sci. Lett.*, *157*, 57–67, 1998.

Helffrich, G., and C. R. Bina, Frequency dependence of the visibility and depths of mantle seismic discontinuities, *Geophys. Res. Lett.*, *21*, 2613–2616, 1994.

Helffrich, G. R., and B. J. Wood, 410 km discontinuity sharpness and the form of the olivine a–b phase diagram: Resolution of apparent seismic contradictions, *Geophys. J. Int.*, *126*, F7–F12, 1996.

Husebye, E. S., R. A. W. Haddon, and D. W. King, Precursors to $P'P'$ and upper mantle discontinuities, *J. Geophys.*, *43*, 535–543, 1977.

Ito, E., and E. Takahashi, Postspinel transformations in the system Mg_2SiO_4-Fe_2SiO_4 and some geophysical implications, *J. Geophys. Res.*, *94*, 10,637–10,646, 1989.

Katsura, T., and E. Ito, The system Mg_2SiO_4-Fe_2SiO_4 at high pressures and temperatures: Precise determination of stabilities of olivine, modified spinel, and spinel, *J. Geophys. Res.*, *94*, 15,663–15,670, 1989.

Melbourne, T., and D. Helmberger, Fine structure of the 410-km discontinuity, *J. Geophys. Res.*, *103*, 10,091–10,102, 1998.

Nakanishi, I., Reflections of $P'P'$ from upper mantle discontinuities beneath the mid-Atlantic ridge, *Geophys. J. R. Astron. Soc.*, *93*, 335–346, 1988.

Niu, F., and H. Kawakatsu, Direct evidence for the undulation of the 660-km discontinuity beneath Tonga: Comparison of Japan and California array data, *Geophys. Res. Lett.*, *22*, 531–534, 1995.

Revenaugh, J., and T. H. Jordan, Mantle layering from *ScS* reverberations, 2, The transition zone, *J. Geophys. Res.*, *96*, 19,763–19,780, 1991a.

Revenaugh, J., and T. H. Jordan, Mantle layering from *ScS* reverberations, 3, The upper mantle, *J. Geophys. Res.*, *96*, 19,781–19,810, 1991b.

Richards, P. G., Seismic waves reflected from velocity gradient anomalies within the Earth's upper mantle, *Z. Geophys.*, *38*, 517–527, 1972.

Ringwood, A. E., Phase transformations in the mantle, *Earth Planet. Sci. Lett.*, *5*, 401–412, 1969.

Shearer, P. M., Global mapping of upper mantle reflectors from long period *SS* precursors, *Geophys. J. Int.*, *115*, 878–904, 1993.

Shearer, P. M., Seismic studies of the upper mantle and transition zone, *U. S. Natl. Rep. Int. Union Geod. Geophys. 1991–1994, Part 1*, *Rev. Geophys.*, *33*, 321–324, 1995.

Shearer, P. M., and M. P. Flanagan, Seismic velocity and density jumps across the 410- and 660-km discontinuities in Earth's upper mantle, *Science*, *285*, 1545–1548, 1999.

Shearer, P. M., and T. G. Masters, Global mapping of topography on the 660-km discontinuity, *Nature*, *355*, 791–796, 1992.

Shen, Z.-K., D. D. Jackson, and B. X. Ge, Crustal deformation across and beyond the Los Angeles basin from geodetic measurements, *J. Geophys. Res.*, *101*, 27,957–27,980, 1996.

Shim, S. H., T. S. Duffy, and G. Shen, The post-spinel transformation in Mg_2SiO_4 and its relation to the 660-km seismic discontinuity, *Nature*, *411*, 571–574, 2001.

Sobel, P. A., The phase P'_dP' as a means for determining upper mantle structure, Ph.D. thesis, 142 pp., Univ. of Minn.-Twin Cities, Minneapolis, 1978.

Stixrude, L., Structure and sharpness of phase transitions and mantle discontinuities, *J. Geophys. Res.*, *102*, 14,835–14,852, 1997.

Vidale, J. E., and H. M. Benz, Upper mantle seismic discontinuities and the thermal structure of subduction zones, *Nature*, *356*, 678–683, 1992.

Vidale, J. E., X.-Y. Ding, and S. P. Grand, The 410-km-depth discontinuity: A sharpness estimate from near-critical reflections, *Geophys. Res. Lett.*, *22*, 2557–2560, 1995.

Walck, M., The *P*-wave upper mantle structure beneath an active spreading center: The Gulf of California, *Geophys. J. R. Astron. Soc.*, *76*, 697–723, 1984.

Warren, L. M., and P. M. Shearer, Investigating the frequency dependence of mantle *Q* by stacking *P* and *PP* spectra, *J. Geophys. Res.*, *105*, 25,391–25,402, 2000.

Whitcomb, J. H., and D. L. Anderson, Reflection of $P'P'$ seismic waves from discontinuities in the mantle, *J. Geophys. Res.*, *75*, 5713–5728, 1970.

Wicks, C. C., and M. A. Richards, A detailed map of the 660-kilometer discontinuity beneath the Izu-Bonin subduction zone, *Science*, *261*, 1424–1427, 1993.

Wood, B. J., The effect of H_2O on the 410-km seismic discontinuity, *Science*, *268*, 74–76, 1995.

P. S. Earle, U. S. Geological Survey, Denver Federal Center, MS966/Box 25046, Denver, CO 80225, USA. (pearle@usgs.gov)

J. E. Vidale and F. Xu, Department of Earth and Space Science, University of California, Los Angeles, Los Angeles, CA 90095-1567, USA. (vidale@ucla.edu; fxu@moho.ess.ucla.edu)